

Intrinsic Superconducting Diode Effect

Akito Daido,¹ Yuhei Ikeda,¹ and Youichi Yanase^{1,2}

¹*Department of Physics, Graduate School of Science, Kyoto University, Kyoto 606-8502, Japan**

²*Institute for Molecular Science, Okazaki 444-8585, Japan*

(Dated: January 12, 2022)

Stimulated by the recent experiment [F. Ando *et al.*, Nature **584**, 373 (2020)], we propose an intrinsic mechanism to cause the superconducting diode effect (SDE). SDE refers to the nonreciprocity of the critical current for the metal-superconductor transition. Among various mechanisms for the critical current, the depairing current is known to be intrinsic to each material and has recently been observed in several superconducting systems. We clarify the temperature scaling of the nonreciprocal depairing current near the critical temperature and point out its significant enhancement at low temperatures. It is also found that the nonreciprocal critical current shows sign reversals upon increasing the magnetic field. These behaviors are understood by the nonreciprocity of the Landau critical momentum and the change in the nature of the helical superconductivity. The intrinsic SDE unveils the rich phase diagram and functionalities of noncentrosymmetric superconductors.

Introduction. — Rectification by the semiconductor diode is one of the central building blocks of electronic devices. Apart from the nonreciprocity induced by asymmetric junctions, it has been revealed that nonreciprocal transport can be obtained as a bulk property of materials [1, 2]. Magnetochiral anisotropy (MCA) [3–13] is an example, described by the equation $R(j) = R_0(1 + \gamma jh)$. Here R , j , and h are the resistance, electric current, and the magnetic field, respectively. The coefficient γ gives rise to different resistance for rightward and leftward electric currents and can be finite in noncentrosymmetric materials. MCA has been observed in (semi)conductors [4–7] as well as in superconductors [10–13], and allows us to access various aspects of noncentrosymmetric materials: from spin-orbit splitting in the band structure [7] to the spin-singlet and -triplet mixing of Cooper pairs [8–10]

MCA is the inequivalence of $R(j)$ and $R(-j)$, where both $R(\pm j)$ usually take finite values. On the other hand, such a drastic situation is possible in superconductors that either one of $R(\pm j)$ vanishes while the other remains finite [Fig. 1]. Such a *superconducting diode effect* (SDE) has recently been observed in the Nb/V/Ta superlattice without an inversion center and is controlled by the applied inplane magnetic field [14]. This is the first report of the SDE in a bulk material, while similar effects have been recognized in engineered systems [15–25] and followed by recent SDE experiments [26, 27]. SDE is a promising building block of the dissipationless electric circuits, and is a fascinating phenomenon manifesting the interplay of the inversion breaking and superconductivity. One of the remaining issues is to identify suitable materials providing the best performance; however, the mechanisms to cause SDE in a bulk material [14] have not been clarified, while the SDE in artificial devices [26, 27] has been well simulated by Bogoliubov-de Gennes (BdG) [26] and time-dependent Ginzburg-Landau (GL) theories [27].

SDE is the nonreciprocity of the critical current for the resistive transition. In usual situations, in particular, under out-of-plane magnetic fields, the resistive transition is caused by the vortex motion. The details of the vortex motion depend on the device setup such as impurity concentrations [28], and in turn, has an advantage of tunability by the nanostruc-

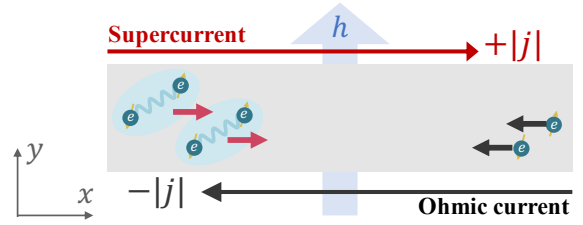


FIG. 1. Schematic figure for the SDE. The system has zero and finite resistance for the rightward and leftward current, respectively, and *vice versa* when the magnetic field h is reversed.

ture engineering [27, 29]. Apart from the extrinsic mechanisms to cause resistivity, the *depairing current* is known as the critical current unique to each superconducting material. Here, the metal-superconductor transition is literally caused by the dissociation of the flowing Cooper pairs [30, 31]. The depairing current always gives the upper limit of the critical current and is an important material parameter characterizing superconductors [28]. The depairing limit generally requires a huge current density, but is within the scope of experimental techniques. Indeed, the depairing limit has recently been achieved in the microbridge superconducting devices of $\text{YBa}_2\text{Cu}_3\text{O}_{7-\delta}$ [32], $\text{Ba}_{0.5}\text{K}_{0.5}\text{Fe}_2\text{As}_2$ [33], and $\text{Fe}_{1+y}\text{Te}_{1-x}\text{Se}_x$ [34].

In this Letter, as a first step of the theoretical research on SDE of bulk materials, we propose the intrinsic mechanism of SDE by studying the nonreciprocity in the depairing current. The results can be tested with the microbridge experiments and establish the foundation of the future study on the bulk SDE. Furthermore, it is revealed that the intrinsic SDE is closely related to the Flude-Ferrell-Larkin-Ovchinnikov state [35, 36]. While the Larkin-Ovchinnikov (LO) state with the spatially inhomogeneous pair potential $\Delta(x) = \Delta \cos qx$ has been discussed for FeSe [37, 38], CeCoIn₅ [39] and organic superconductors [40], the Flude-Fellel (FF) type order parameter $\Delta(x) = \Delta e^{iqx}$ is known to ubiquitously appear in noncentrosymmetric superconductors and is particularly called the *helical superconductivity* [41–53]. Implications of

the helical superconductivity have been obtained in thin films of Pb [52] and doped SrTiO₃ [54], and a heavy-fermion superlattice [55, 56]. We show that the intrinsic SDE works as a probe to study the phase diagram of helical superconductivity. Relation to the recent experiments [14, 57] is also discussed.

Model. — We consider the critical current in two-dimensional (2D) superconductors with a polar axis due to the substrate and/or the crystal structure. The magnetic field is applied along the y direction, which makes the critical current nonreciprocal in the x direction [Fig. 1]. The system is modeled by the Rashba-Zeeman Hamiltonian with the attractive Hubbard interaction,

$$\hat{H} = \sum_{\mathbf{k}\sigma\sigma'} [\xi(\mathbf{k})\delta_{\sigma\sigma'} + \mathbf{g}(\mathbf{k}) \cdot \boldsymbol{\sigma}_{\sigma\sigma'} - h(\sigma_y)_{\sigma\sigma'}] c_{\mathbf{k}\sigma}^\dagger c_{\mathbf{k}\sigma'} - \frac{U}{V} \sum_{\mathbf{k}_1+\mathbf{k}_2+\mathbf{k}_3+\mathbf{k}_4=0} c_{\mathbf{k}_1\uparrow}^\dagger c_{\mathbf{k}_2\downarrow}^\dagger c_{\mathbf{k}_3\downarrow} c_{\mathbf{k}_4\uparrow}. \quad (1)$$

Here, $\xi(\mathbf{k}) = -2t_1(\cos k_x + \cos k_y) + 4t_2 \cos k_x \cos k_y - \mu$ and $\mathbf{g}(\mathbf{k}) = \alpha_g(-\sin k_y, \sin k_x, 0)$ represent the hopping energy and the Rashba spin-orbit coupling, respectively. The magnetic field in the y direction is introduced by the Zeeman term $h \equiv \mu_B H_y$. The parameters are given by $(t_1, t_2, \mu, \alpha_g, U) = (1, 0, -1, 0.3, 1.5)$ unless mentioned otherwise. The next-nearest-neighbor hopping t_2 is introduced for the latter use. The energy dispersion of the noninteracting part is given by $\xi_\chi^h(\mathbf{k}) = \xi(\mathbf{k}) + \chi|\mathbf{g}(\mathbf{k}) - h\hat{y}| \simeq \xi_\chi^0(\mathbf{k} - \mathbf{q}_\chi(\mathbf{k})/2)$. Here, each band is labeled by the helicity $\chi = \pm$, and the momentum shift under h is given by $\mathbf{q}_\chi(\mathbf{k})/2 = \chi g_y(\mathbf{k}) h v_\chi(\mathbf{k}) / |v_\chi(\mathbf{k})|^2$ with $v_\chi(\mathbf{k}) \equiv \nabla \xi_\chi^0(\mathbf{k})$. The momentum shift is estimated by its Fermi-surface (FS) average, $q_\chi \equiv \hat{x} \cdot \langle \mathbf{q}_\chi(\mathbf{k}) \rangle_{\text{FS}} \sim 2\chi h / \langle |v_\chi(\mathbf{k})| \rangle_{\text{FS}}$.

We solve the model (1) within the mean-field approximation. The attractive Hubbard interaction is approximated by

$$\frac{1}{2} \sum_{\mathbf{k}\sigma\sigma'} \Delta (i\sigma_y)_{\sigma\sigma'} c_{\mathbf{k}+\mathbf{q}\sigma}^\dagger c_{-\mathbf{k}\sigma'}^\dagger + \text{H.c.} + \Delta^2/2U. \quad (2)$$

The s -wave pair potential Δ is considered with a center-of-mass momentum $\mathbf{q} = q\hat{x}$ to describe the current-flowing state. For a given q , the value of $\Delta = \Delta(q)$ is determined self-consistently by the gap equation with the temperature T . To describe the superconducting transitions and the supercurrent, it is convenient to introduce the condensation energy $F(q)$ for each q , that is, the difference of the free energy per unit area in the normal and superconducting states. The sheet current density is obtained by $j(q) = 2\partial_q F(q)$, which coincides with the expectation value of the current operator [58].

When an electric current j_{ex} is applied, the superconducting state with q satisfying $j(q) = j_{\text{ex}}$ should be realized. However, no superconducting state can sustain j_{ex} when $j_{\text{ex}} < j_{c-}$ or $j_{\text{ex}} > j_{c+}$, with $j_{c+} \equiv \max_q j(q)$ and $j_{c-} \equiv \min_q j(q)$. Thus, the depairing current in the positive and negative directions is given by the maximum j_{c+} and minimum j_{c-} of $j(q)$, respectively. In particular, the nonreciprocal component is given by

$$\Delta j_c \equiv j_{c+} + j_{c-} = j_{c+} - |j_{c-}|. \quad (3)$$

The SDE is identified with a finite Δj_c of the system. We also define the averaged critical current $\bar{j}_c \equiv (j_{c+} - j_{c-})/2$, by which the strength of the nonreciprocal nature can be expressed as $r \equiv \Delta j_c / \bar{j}_c$.

GL analysis. — First, we discuss the SDE by the GL theory. The GL free energy $f(\Delta, q) = \alpha(q)\Delta^2 + \frac{\beta(q)}{2}\Delta^4$ gives a good approximation of $F(q)$ near the transition temperature T_c when the optimized order parameter $\Delta = \Delta(q)$ is substituted. The GL coefficients are assumed to have the following form: $\alpha(q) = \alpha_0 + \alpha_1 q + \frac{1}{2}\alpha_2 q^2 + \frac{1}{6}\alpha_3 q^3$, and $\beta(q) = \beta_0 + \beta_1 q$, which is valid for the description up to $O(T_c - T)^{5/2}$. When the higher-order gradient terms α_3, β_1 are neglected, the broken inversion and time-reversal symmetries are encoded solely into $\alpha_1 \neq 0$, which shifts the minimum of $f(q) = f(\Delta(q), q)$ from $q = 0$ to $q_0 = -\alpha_1/2\alpha_2$. Thus, the superconducting state with a finite q_0 , namely the helical superconductivity is realized [42, 43]. The helical superconducting state with $q = q_0$ does not carry a supercurrent [43, 45, 48], $j(q_0) = 2\partial_{q_0} f(q_0) = 0$, as the most stable state generally should be.

It is convenient to rewrite the GL coefficients as $\alpha(q) = \tilde{\alpha}_0 + \frac{\tilde{\alpha}_2}{2}(q - \tilde{q}_0)^2 + \frac{\alpha_3}{6}(q - \tilde{q}_0)^3$ and $\beta(q) = \tilde{\beta}_0 + \beta_1(q - \tilde{q}_0)$, where the linear term in $\alpha(q)$ is erased. Clearly, $f(\Delta, q + \tilde{q}_0)$ for $\alpha_3 = \beta_1 = 0$ is equivalent to the GL free energy of a centrosymmetric superconductor, leading to a reciprocal critical current [42]. Thus, the SDE is caused by the higher-order terms, α_3 and β_1 ,

$$\Delta j_c = \left(\frac{16}{27\tilde{\beta}_0\tilde{\alpha}_2} \alpha_3 - \frac{8}{9\tilde{\beta}_0^2} \beta_1 \right) \tilde{\alpha}_0^2, \quad (4)$$

up to first order in α_3 and β_1 [58]. Note that $\Delta j_c \propto (T_c - T)^2$ in contrast to the averaged critical current $\bar{j}_c \propto (T_c - T)^{3/2}$ [30, 58], since $\tilde{\alpha}_0 \propto T - T_c$. Thus, a small but finite Δj_c is predicted by the GL theory, while a larger Δj_c is expected at low temperatures. The result obtained here is valid for general noncentrosymmetric superconductors without orbital depairing effect, e.g., superconducting thin films under inplane magnetic fields.

Critical current under low fields. — Equipped with the insight of the GL theory, we discuss the temperature dependence of Δj_c based on the model (1). The result is shown in Fig. 2 for $h = 0.03$. As shown in the inset, the temperature scaling $\Delta j_c \propto (T_c - T)^2$ is confirmed near the transition temperature T_c . The scaling law becomes inaccurate as $T_c - T$ gets large, where $\Delta(T)$ also deviates from $\Delta(T) \propto \sqrt{T_c - T}$. Importantly, $\Delta j_c(T)$ is strongly enhanced at low temperatures.

To clarify the origin of the SDE, we show $j(q)$ by red lines in Figs. 3. In Fig. 3 (a) for $T = 0.03 \simeq T_c$, $j(q)$ is a smooth curve and its tiny asymmetry gives rise to Δj_c , as is illustrated by the difference of the solid and dashed horizontal lines (indicating j_{c+} and $-j_{c-}$). This is consistent with the GL picture where Δj_c is caused by the asymmetry factors $\alpha_3, \beta_1 \neq 0$. Two curves, $j(q)$ and $-j(q)$, cross at $q_0 < 0$, indicating the helical superconductivity. In Fig. 3 (c), $\Delta(q)$ and the minimum excitation energy $\Delta E(q)$ are shown in addition to $j(q)$,

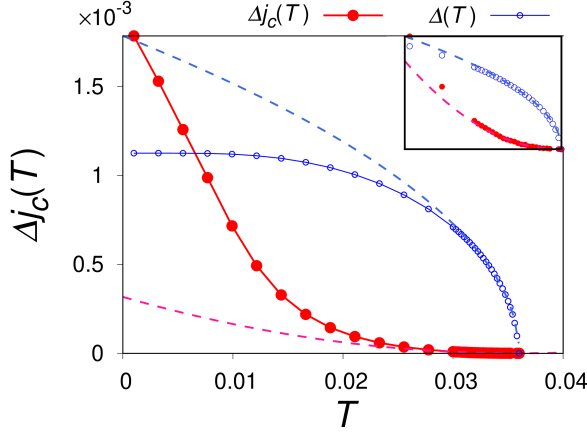


FIG. 2. The temperature dependence of Δj_c at $h = 0.03$. The red closed circles indicate $\Delta j_c(T)$, while the open blue circles indicate $\Delta(T)$ (a.u.). The dashed lines show the fitting curve of $\Delta j_c(T)$ and $\Delta(T)$ near T_c with $(T_c - T)^2$ and $\sqrt{T_c - T}$, respectively. The inset shows the enlarged figure near $T_c \approx 0.036$.

by the blue and black lines, respectively. The superconducting state remains stable even after the spectrum becomes gapless, and reaches the maximum and minimum of $j(q)$ in the gapless region.

As shown in Fig. 3 (b), the dispersion of $j(q)$ at $T = 0.001 \ll T_c$ is significantly different from that at $T = 0.03$, and a large Δj_c is realized. The maximum and minimum of $j(q)$ are achieved at the ends of the region where $j(q)$ is almost linear in q . These momenta approximately coincide with the Landau critical momenta, $q_R > 0$ and $q_L < 0$, i.e. the first q 's satisfying $\Delta E(q) = 0$, as is clear from Fig. 3 (d). Actually, the depairing effect takes place after $q > q_R$ or $q < q_L$: The excited quasiparticles reduce $|j(q)|$ and $\Delta(q)$ and finally cause a first-order phase transition into the normal state. From these observations, we obtain the formula

$$\Delta j_c = n_{xx}^s (q_R + q_L - 2q_0)/2, \quad (5)$$

by using, e.g., $j_{c+} = n_{xx}^s (q_R - q_0)/2$ with the superfluid weight $n_{xx}^s = 2\partial_{q_0} j(q_0)$. Thus, the nonreciprocal Landau critical momentum $q_R + q_L$ measured from $2q_0$ gives rise to the SDE at extremely low temperatures. As T gets larger, the maximum and minimum of $j(q)$ deviate from $j(q_R)$ and $j(q_L)$, and Eq. (5) becomes no longer valid. The mechanism of the SDE at low temperatures is not captured by the GL theory.

Phase diagram. — In Figs. 4 (a) and (b), we show the temperature and magnetic-field dependence of the nonreciprocal component Δj_c for $t_2 = 0$ and $t_2 = 0.2$. Let us focus on the low-field region, where positive and negative values of Δj_c are widely obtained for Fig. 4 (a) and (b), respectively. The sign reversal of Δj_c by t_2 can be understood based on Eq. (5). Indeed, we show in the Supplemental Material [58] that $q_R + q_L - 2q_0$ causes a sign reversal as t_2 increases, leading to that of Δj_c as well. It is also shown that for large values

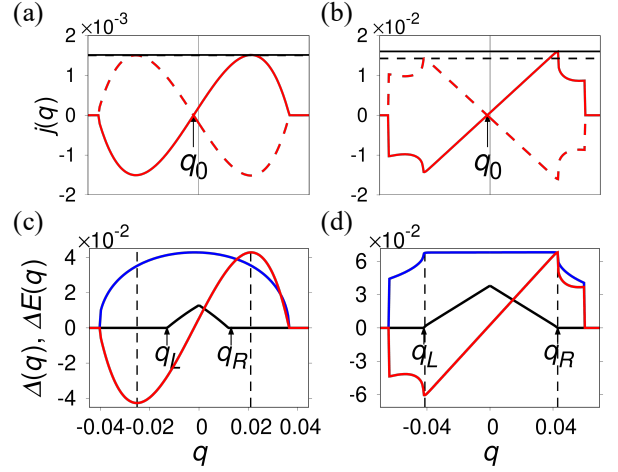


FIG. 3. (a), (b): The q dependence of the supercurrent at $h = 0.03$ and (a) $T = 0.03$ and (b) $T = 0.001$. In addition to $j(q)$ (red lines), $-j(q)$ (dashed red lines) is shown. The black (dashed) horizontal lines indicate j_{c+} ($-j_{c-}$). The position of q_0 is indicated by arrows. (c), (d): The order parameter $\Delta(q)$ (blue lines) and the excitation gap $\Delta E(q)$ (black lines) are shown together with $j(q)$ (a.u.). The parameters for the panels (c) and (d) are the same as the panel (a) and (b), respectively. The vertical dashed black lines indicate the momentum q where $j(q) = j_{c\pm}$. Landau critical momenta q_R and q_L are indicated by arrows.

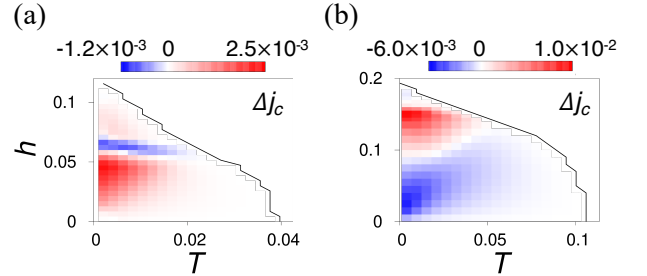


FIG. 4. The magnetic-field and temperature dependence of the nonreciprocal component of the critical current $\Delta j_c(h, T)$ for (a) $t_2 = 0$ and (b) $t_2 = 0.2$. The red and blue colors indicate positive and negative values of Δj_c , respectively. The transition temperature $T_c(h)$ determined with the T mesh (a) 0.045/21 and (b) 0.12/21 is shown with the black line for the guide of the eye.

of t_2 , $q_R + q_L - 2q_0$ is dominated by the nonreciprocal Landau critical momentum $q_R + q_L$, while it is dominated by $-2q_0$ for small values of t_2 . A relatively large SDE for $t_2 \sim 0.2$ is explained by large values of $q_R + q_L - 2q_0$ as a result of the anisotropy [58]. The pronounced aspect of Fig. 4 is the sign reversals prevailing under moderate and high magnetic fields. This point will be discussed in the following.

Critical current under high fields. — To see the origin of the high-field behavior, we show the condensation energy $F(q)$ at $T = 0.001$ for various values of h in Fig. 5. To be specific, the case of Fig. 4 (a) is considered. The condensation energy $F(q)$ shown by the blue line has a single-well

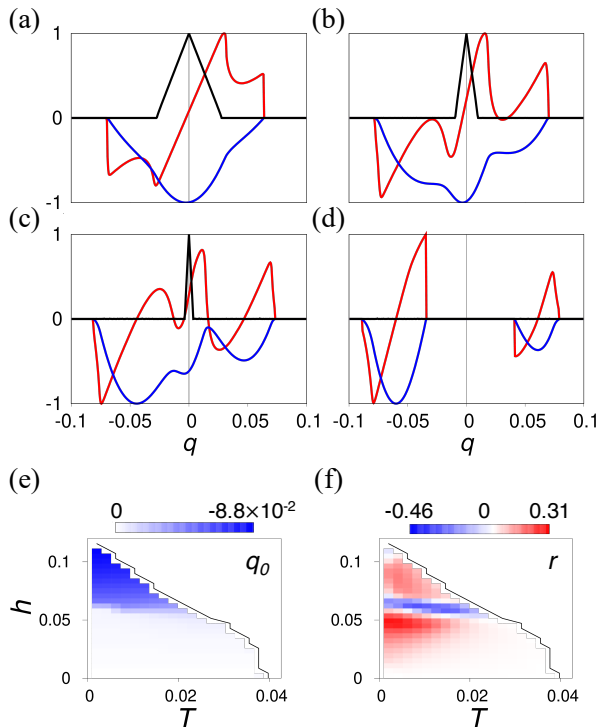


FIG. 5. (a)-(d) $j(q)$ (red lines), $F(q)$ (blue lines), and $\Delta E(q)$ (black lines) normalized to $[-1, 1]$ at $T = 0.001$ for (a) $h = 0.043$, (b) $h = 0.058$, (c) $h = 0.063$ and (d) $h = 0.075$. (e),(f) q_0 and r for various values of h and T .

structure under low magnetic fields [panel (a)]. The structure near $|q| \sim 0.05$ is developed under higher magnetic fields [panel (b)], to form two local minima [panel (c)], where the left one becomes most stable. These side wells are the precursor of the high-field helical superconducting states [panel (d)], where the central minimum finally disappears. Such a change is most evident in $q_0(T, h)$ shown in Fig. 5 (e). Under low fields, q_0 is determined by the balance of two Fermi surfaces shifted in the opposite directions, resulting in $|q_0| \lesssim 10^{-2}$; on the other hand, under high fields, $q_0 \sim 10^{-1}$ almost coincides with q_χ of the Fermi surface with a larger density of states [42, 45, 47, 50]. This determines the “crossover line” [59] of helical superconductivity visible at $h \sim 0.06$ in Fig. 5 (e).

The evolution of $j(q)$ by h follows that of $F(q)$. Overall, $j(q)$ consists of several almost-straight lines and their interpolation, since $F(q)$ is approximated by the square function of q around each local minimum. Comparing Figs. 5 (a) and (b), the q point achieving j_{c-} is changed from q_L to a critical momentum of the left well, which we name $q_{-,L}$. In the panel (c), $q_{-,L}$ remains to give j_{c-} , whose value is significantly enhanced owing to the development of the left minimum. This causes the sign reversal of Δj_c . In the panel (d), Δj_c is determined by the tiny asymmetry of the left well. It should be noticed that the ratio $r = \Delta j_c / \bar{j}_c$ shown in Fig. 5 (f) is quite large around the crossover line, takes values up to $|r| \lesssim 0.4$,

as is understood from Figs. 5 (a)-(c). Thus, the sign reversals and huge values of $r = \Delta j_c / \bar{j}_c$ under magnetic fields are caused by the change in the helical superconducting states. According to Figs. 5 (e) and (f), the sign reversal also occurs near $T_c(h)$ by the crossover.

Figure 4 (b) can be understood similarly. In this case, the crossover line is identified to be $h \sim 0.17$ [58], where Δj_c changes its sign. The high-field helical superconducting states span only a small fraction in the phase diagram. The difference from Fig. 4 (a) is another sign reversal at $h \sim 0.09$. In this region, Δj_c is determined by the nonreciprocal Landau critical momentum, and $q_R + q_L - 2q_0$ turns out to change its sign by increasing h . This is because $q_R + q_L (< 0)$ shows nonmonotonic behavior, while $-2q_0 (> 0)$ grows linearly and finally becomes dominant [58]. The sign reversal survives at higher temperatures and reaches the transition temperature.

Discussion — We have revealed the sign reversals of the SDE, which is closely connected with the change in the helical superconducting states. Thus, the intrinsic SDE is a promising bulk probe directly unveiling the crossover line. This probe is complementary to the junction [46] and spectroscopy [42] experiments proposed to detect the helical superconductivity.

In the end, we briefly discuss the connection with the experimental results of SDE [14]. The sign reversals of Δj_c by increasing the magnetic field at low temperatures have recently been observed [57], which might be explained by our results for the intrinsic SDE. An “inverse effect,” the nonreciprocity of the critical magnetic field under applied electric current, has also been reported [60], implying the nonreciprocity as a bulk property of the superconductor. Thus, the SDE with sign reversals implies the crossover in the superconducting state of the Nb/V/Ta superlattice. On the other hand, $\Delta j_c(h)$ near T_c seems to be at variance with the intrinsic SDE [14]. This point might be overcome by considering the effect of vortices, which is left as an intriguing future issue.

We appreciate helpful discussions with T. Ono, Y. Miyasaka, R. Kawarazaki, H. Narita, and H. Watanabe. This work was supported by JSPS KAKENHI (Grants No. JP18H05227, No. JP18H01178, No. 20H05159, No. 21K13880, and No. 21J14804), JSPS research fellowship, WISE Program MEXT, and SPIRITS 2020 of Kyoto University.

Note added.— During finalizing the manuscript, we became aware of independent overlapping works. A recent arXiv post by N. Yuan and L. Fu [61] studies the depairing current of the Rashba-Zeeman model mainly using the GL theory. However, sign reversals of the SDE are not obtained. The work by J. He and N. Nagaosa *et al.* [62] studies the related topic independently of ours. We thank J. He for coordinating submission to arXiv.

* daido@scphys.kyoto-u.ac.jp

[1] Y. Tokura and N. Nagaosa, Nat. Commun. **9**, 3740 (2018).

- [2] T. Ideue and Y. Iwasa, *Annu. Rev. Condens. Matter Phys.* **12**, 201 (2021).
- [3] G. L. Rikken, J. Fölling, and P. Wyder, *Phys. Rev. Lett.* **87**, 236602 (2001).
- [4] V. Krstić, S. Roth, M. Burghard, K. Kern, and G. L. J. A. Rikken, *J. Chem. Phys.* **117**, 11315 (2002).
- [5] F. Pop, P. Auban-Senzier, E. Canadell, G. L. J. A. Rikken, and N. Avarvari, *Nat. Commun.* **5**, 3757 (2014).
- [6] G. L. J. A. Rikken and P. Wyder, *Phys. Rev. Lett.* **94**, 016601 (2005).
- [7] T. Ideue, K. Hamamoto, S. Koshikawa, M. Ezawa, S. Shimizu, Y. Kaneko, Y. Tokura, N. Nagaosa, and Y. Iwasa, *Nat. Phys.* **13**, 578 (2017).
- [8] R. Wakatsuki and N. Nagaosa, *Phys. Rev. Lett.* **121**, 026601 (2018).
- [9] S. Hoshino, R. Wakatsuki, K. Hamamoto, and N. Nagaosa, *Phys. Rev. B Condens. Matter* **98**, 054510 (2018).
- [10] R. Wakatsuki, Y. Saito, S. Hoshino, Y. M. Itahashi, T. Ideue, M. Ezawa, Y. Iwasa, and N. Nagaosa, *Science Advances* **3**, e1602390 (2017).
- [11] F. Qin, W. Shi, T. Ideue, M. Yoshida, A. Zak, R. Tenne, T. Kikitsu, D. Inoue, D. Hashizume, and Y. Iwasa, *Nat. Commun.* **8**, 14465 (2017).
- [12] K. Yasuda, H. Yasuda, T. Liang, R. Yoshimi, A. Tsukazaki, K. S. Takahashi, N. Nagaosa, M. Kawasaki, and Y. Tokura, *Nat. Commun.* **10**, 2734 (2019).
- [13] Y. M. Itahashi, T. Ideue, Y. Saito, S. Shimizu, T. Ouchi, T. Nojima, and Y. Iwasa, *Science advances* **6**, eaay9120 (2020).
- [14] F. Ando, Y. Miyasaka, T. Li, J. Ishizuka, T. Arakawa, Y. Shiota, T. Moriyama, Y. Yanase, and T. Ono, *Nature* **584**, 373 (2020).
- [15] A. A. Reynoso, G. Usaj, C. A. Balseiro, D. Feinberg, and M. Avignon, *Phys. Rev. Lett.* **101**, 107001 (2008).
- [16] A. Zazunov, R. Egger, T. Jonckheere, and T. Martin, *Phys. Rev. Lett.* **103**, 147004 (2009).
- [17] I. Margaritis, V. Paltoglou, and N. Flytzanis, *J. Phys. Condens. Matter* **22**, 445701 (2010).
- [18] T. Yokoyama, M. Eto, and Y. V. Nazarov, *Phys. Rev. B Condens. Matter* **89**, 195407 (2014).
- [19] M. A. Silaev, A. Y. Aladyshkin, M. V. Silaeva, and A. S. Aladyshkina, *J. Phys. Condens. Matter* **26**, 095702 (2014).
- [20] G. Campagnano, P. Lucignano, D. Giuliano, and A. Tagliacozzo, *J. Phys. Condens. Matter* **27**, 205301 (2015).
- [21] F. Dolcini, M. Houzet, and J. S. Meyer, *Phys. Rev. B Condens. Matter* **92**, 035428 (2015).
- [22] C.-Z. Chen, J. J. He, M. N. Ali, G.-H. Lee, K. C. Fong, and K. T. Law, *Phys. Rev. B Condens. Matter* **98**, 075430 (2018).
- [23] M. Minutillo, D. Giuliano, P. Lucignano, A. Tagliacozzo, and G. Campagnano, *Phys. Rev. B Condens. Matter* **98**, 144510 (2018).
- [24] S. Pal and C. Benjamin, *EPL* **126**, 57002 (2019).
- [25] A. A. Kopusov, A. G. Kutlin, and A. S. Mel'nikov, *Phys. Rev. B Condens. Matter* **103**, 144520 (2021).
- [26] C. Baumgartner, L. Fuchs, A. Costa, S. Reinhardt, S. Gronin, G. C. Gardner, T. Lindemann, M. J. Manfra, P. E. Faria Junior, D. Kochan, J. Fabian, N. Paradiso, and C. Strunk, *Nat. Nanotechnol.*, 10.1038/s41565 (2021).
- [27] Y.-Y. Lyu, J. Jiang, Y.-L. Wang, Z.-L. Xiao, S. Dong, Q.-H. Chen, M. V. Milošević, H. Wang, R. Divan, J. E. Pearson, P. Wu, F. M. Peeters, and W.-K. Kwok, *Nat. Commun.* **12**, 2703 (2021).
- [28] G. Blatter, M. V. Feigel'man, V. B. Geshkenbein, A. I. Larkin, and V. M. Vinokur, *Rev. Mod. Phys.* **66**, 1125 (1994).
- [29] J. E. Villegas, S. Savel'ev, F. Nori, E. M. Gonzalez, J. V. Anguita, R. García, and J. L. Vicent, *Science* **302**, 1188 (2003).
- [30] M. Tinkham, *Introduction to Superconductivity* (Courier Corporation, 2004).
- [31] D. Dew-Hughes, *Low Temp. Phys.* **27**, 713 (2001).
- [32] S. Nawaz, R. Arpaia, F. Lombardi, and T. Bauch, *Phys. Rev. Lett.* **110**, 167004 (2013).
- [33] J. Li, J. Yuan, Y.-H. Yuan, J.-Y. Ge, M.-Y. Li, H.-L. Feng, P. J. Pereira, A. Ishii, T. Hatano, A. V. Silhanek, L. F. Chibotaru, J. Vanacken, K. Yamaura, H.-B. Wang, E. Takayama-Muromachi, and V. V. Moshchalkov, *Appl. Phys. Lett.* **103**, 062603 (2013).
- [34] Y. Sun, H. Ohnuma, S.-Y. Ayukawa, T. Noji, Y. Koike, T. Tamegai, and H. Kitano, *Phys. Rev. B* **101**, 134516 (2020).
- [35] A. I. Larkin and Y. N. Ovchinnikov, *Zh. Eksperim. i Teor. Fiz.* **47**, 1136 (1964).
- [36] P. Fulde and R. A. Ferrell, *Phys. Rev.* **135**, A550 (1964).
- [37] S. Kasahara, T. Watashige, T. Hanaguri, Y. Kohsaka, T. Yamashita, Y. Shimoyama, Y. Mizukami, R. Endo, H. Ikeda, K. Aoyama, T. Terashima, S. Uji, T. Wolf, H. von Löhneysen, T. Shibauchi, and Y. Matsuda, *Proc. Natl. Acad. Sci. U. S. A.* **111**, 16309 (2014).
- [38] S. Kasahara, Y. Sato, S. Licciardello, M. Čulo, S. Arsenijević, T. Ottenbros, T. Tominaga, J. Böker, I. Eremin, T. Shibauchi, J. Wosnitzer, N. E. Hussey, and Y. Matsuda, *Phys. Rev. Lett.* **124**, 107001 (2020).
- [39] Y. Matsuda and H. Shimahara, *J. Phys. Soc. Jpn.* **76**, 051005 (2007).
- [40] J. Wosnitzer, *Ann. Phys.* **530**, 1700282 (2018).
- [41] E. Bauer and M. Sigrist, *Non-Centrosymmetric Superconductors: Introduction and Overview* (Springer Science & Business Media, 2012).
- [42] M. Smidman, M. B. Salamon, H. Q. Yuan, and D. F. Agterberg, *Rep. Prog. Phys.* **80**, 036501 (2017).
- [43] D. F. Agterberg, *Physica C Supercond.* **387**, 13 (2003).
- [44] V. Barzykin and L. P. Gor'kov, *Phys. Rev. Lett.* **89**, 227002 (2002).
- [45] O. V. Dimitrova and M. V. Feigel'man, *JETP Lett.* **78**, 637 (2003).
- [46] R. P. Kaur, D. F. Agterberg, and M. Sigrist, *Phys. Rev. Lett.* **94**, 137002 (2005).
- [47] D. F. Agterberg and R. P. Kaur, *Phys. Rev. B Condens. Matter* **75**, 064511 (2007).
- [48] O. Dimitrova and M. V. Feigel'man, *Phys. Rev. B Condens. Matter* **76**, 014522 (2007).
- [49] K. V. Samokhin, *Phys. Rev. B Condens. Matter* **78**, 224520 (2008).
- [50] Y. Yanase and M. Sigrist, *J. Phys. Soc. Jpn.* **77**, 342 (2008).
- [51] K. Michaeli, A. C. Potter, and P. A. Lee, *Phys. Rev. Lett.* **108**, 117003 (2012).
- [52] T. Sekihara, R. Masutomi, and T. Okamoto, *Phys. Rev. Lett.* **111**, 057005 (2013).
- [53] M. Houzet and J. S. Meyer, *Phys. Rev. B Condens. Matter* **92**, 014509 (2015).
- [54] T. Schumann, L. Galletti, H. Jeong, K. Ahadi, W. M. Strickland, S. Salmani-Rezaie, and S. Stemmer, *Phys. Rev. B Condens. Matter* **101**, 100503 (2020).
- [55] M. Naritsuka, T. Ishii, S. Miyake, Y. Tokiwa, R. Toda, M. Shimozaawa, T. Terashima, T. Shibauchi, Y. Matsuda, and Y. Kasahara, *Phys. Rev. B Condens. Matter* **96**, 174512 (2017).
- [56] M. Naritsuka, T. Terashima, and Y. Matsuda, *J. Phys. Condens. Matter* **33**, 273001 (2021).
- [57] T. Ono, Y. Miyasaka, and R. Kawarazaki, Private communication.
- [58] See Supplemental Material for more details.
- [59] This terminology is named after the crossover generally seen in

noncentrosymmetric superconductors, while the line changes to the first-order transition at lower temperature $T \lesssim 0.12$ in this model, as in Figs.5(b)-5(d).

- [60] Y. Miyasaka, R. Kawarazaki, H. Narita, F. Ando, Y. Ikeda, R. Hisatomi, A. Daido, Y. Shiota, T. Moriyama, Y. Yanase, and T. Ono, *Appl. Phys. Express* **14**, 073003 (2021).
 [61] N. F. Q. Yuan and L. Fu, (2021), [arXiv:2106.01909 \[cond-mat.supr-con\]](#).
 [62] J. J. He, Y. Tanaka, and N. Nagaosa, "A phenomenological theory of superconductor diodes in presence of magnetochiral anisotropy," (2021), [arXiv:2106.03575 \[cond-mat.supr-con\]](#).

FORMULATION TO EVALUATE THE ELECTRIC CURRENT

Here, we show the details of the formulation to calculate the current expectation values in the superconducting states. The free energy per unit volume in the superconducting state is given by

$$\begin{aligned} \Omega(\Delta, q) &\equiv -\frac{T}{V} \ln \text{Tr} e^{-\hat{H}_{\text{MF}}^q(\Delta)/T} \\ &= \frac{1}{2V} \sum_{\mathbf{k}} \text{tr}_N \left[\frac{\Delta^2}{U} + H_N(\mathbf{k}) \right] \\ &\quad - \frac{T}{2V} \sum_{\mathbf{k}} \text{tr} \left[\ln(1 + e^{-H(\mathbf{k}, q)/T}) \right]. \end{aligned} \quad (6)$$

Here, tr_N represents the trace over the spin degrees of freedom, while tr represents that over both the spin and the Nambu degrees of freedom. $V = L_x L_y$ represents the system size with L_i the diameter in the $i = x, y$ direction. We introduced the Bogoliubov-de Genens (BdG) Hamiltonian $H(\mathbf{k}, q)$ by

$$\begin{aligned} \hat{H}_{\text{MF}}^q(\Delta) &= \frac{1}{2} \sum_{\mathbf{k}} \Psi^\dagger(\mathbf{k}, q) H(\mathbf{k}, q) \Psi(\mathbf{k}, q) + \text{const.}, \quad (7) \\ H(\mathbf{k}, q) &= \begin{pmatrix} H_N(\mathbf{k} + \mathbf{q}) & \Delta i \sigma_y \\ -\Delta i \sigma_y & -H_N^T(-\mathbf{k}) \end{pmatrix}, \quad (8) \end{aligned}$$

with the momentum $\mathbf{q} = q\hat{x}$ and the Nambu spinor $\Psi(\mathbf{k}, q)^\dagger = (c_{\mathbf{k}+\mathbf{q}\uparrow}^\dagger, c_{\mathbf{k}+\mathbf{q}\downarrow}^\dagger, c_{-\mathbf{k}\uparrow}, c_{-\mathbf{k}\downarrow})$. Here, we choose q to be compatible with the periodic boundary conditions, $q \in 2\pi\mathbb{Z}/L_x$. The constant term in Eq. (7) is equivalent to the first term of Eq. (6). The normal-state Bloch Hamiltonian is given by $H_N(\mathbf{k}) = \xi(\mathbf{k}) + (\mathbf{g}(\mathbf{k}) - \mathbf{h}) \cdot \boldsymbol{\sigma}$.

The electric current (the sheet current density) is defined by

$$j(\Delta, q) = \frac{\text{tr} [\hat{j}_x e^{-\hat{H}_{\text{MF}}^q(\Delta)/T}]}{\text{tr} [e^{-\hat{H}_{\text{MF}}^q(\Delta)/T}]}. \quad (9)$$

Here, the current operator is given by

$$\hat{j}_x = \frac{1}{V} \sum_{\mathbf{k}\sigma\sigma'} \partial_{k_x} H_N(\mathbf{k})_{\sigma\sigma'} c_{\mathbf{k}\sigma}^\dagger c_{\mathbf{k}\sigma'} \quad (10)$$

$$= \frac{1}{V} \sum_{\mathbf{k}} \Psi^\dagger(\mathbf{k}, q) \partial_q H(\mathbf{k}, q) \Psi(\mathbf{k}, q). \quad (11)$$

After some calculations, we obtain

$$j(\Delta, q) = \frac{1}{V} \sum_{\mathbf{k}} \text{tr} [\partial_q H(\mathbf{k}, q) f(H(\mathbf{k}, q))] \quad (12)$$

$$= 2\partial_q \Omega(\Delta, q), \quad (13)$$

with the Fermi distribution function $f(\epsilon) = (e^{\epsilon/T} + 1)^{-1}$.

The gap equation is given by

$$\partial_\Delta \Omega(\Delta, q) = 0, \quad (14)$$

which determines the pair potential Δ self-consistently. The solution is written as $\Delta(q)$, and satisfies Eq. (14), or equivalently,

$$\Delta(q) = -\frac{U}{V} \sum_{\mathbf{k}} \langle c_{-\mathbf{k}\downarrow} c_{\mathbf{k}+\mathbf{q}\uparrow} \rangle |_{\Delta=\Delta(q)}. \quad (15)$$

By using $\Delta(q)$, the condensation energy defined in the main text is written as

$$F(q) = \Omega(\Delta(q), q) - \Omega(0, q), \quad (16)$$

where $\Omega(0, q) = \Omega(0, 0)$ holds as is easily confirmed with Eqs. (6) and (8). By using Eqs. (13) and (14), we obtain

$$\begin{aligned} 2\partial_q F(q) &= \lim_{\Delta \rightarrow \Delta(q)} [2\partial_q \Omega(\Delta, q) + 2\partial_q \Delta(q) \partial_\Delta \Omega(\Delta, q)] \\ &= j(\Delta(q), q) \\ &\equiv j(q). \end{aligned} \quad (17)$$

The obtained equality goes along with the standard expression $j = -\partial_A \Omega$ with A the uniform vector potential since q changes by $-2\delta A$ when A changes by δA .

GL ANALYSIS

Here we show the details of the GL analysis of the superconducting diode effect. Let us start from the expression

$$f(\Delta, q) = \alpha(q) \Delta^2 + \frac{\beta(q)}{2} \Delta^4, \quad (18)$$

keeping the order parameter of the form $\Delta(x) \propto e^{iqx}$ in mind. The coefficients are given by

$$\begin{aligned} \alpha(q) &= -\tilde{\alpha}_0 + \frac{\tilde{\alpha}_2}{2} (q - q_0)^2 + \frac{\alpha_3}{6} (q - q_0)^3, \\ \beta(q) &= \tilde{\beta}_0 + \beta_1 (q - q_0). \end{aligned} \quad (19)$$

Here we omit the tilde of \tilde{q}_0 in the main text for simplicity, and redefine $\tilde{\alpha}_0 \rightarrow -\tilde{\alpha}_0$. The order parameter is optimized by

$$\partial f / \partial \Delta^2 = \alpha(q) + \beta(q) \Delta^2 = 0. \quad (20)$$

Assuming $\beta(q) > 0$ for the range of q we are interested in, Δ has a nontrivial real solution only when $\alpha(q) < 0$. Thus, the GL free energy is given by

$$f(q) = f(\Delta(q), q) = -\frac{\alpha(q)^2}{2\beta(q)} \theta(-\alpha(q)), \quad (21)$$

with $\theta(x)$ the Heaviside step function. Since the minimum of $\alpha(q)$ is $-\tilde{\alpha}_0$, the transition from the normal to helical superconducting state occurs when the sign of $\tilde{\alpha}_0$ changes from negative to positive as lowering the temperature. Thus, we conclude $\tilde{\alpha}_0 \propto T_c - T$.

We first consider the case $\alpha_3 = \beta_1 = 0$. The supercurrent is given by $j(q) = 2\partial_q f(q)$,

$$\tilde{\beta}_0 j(q)/2 = -\partial_q \alpha(q)^2/2 = -\alpha(q)\partial_q \alpha(q). \quad (22)$$

This is an odd function of $q - q_0$, and thus the critical current is reciprocal. Actually, The maximum and minimum of $j(q)$ are achieved at $q = q_c$ satisfying

$$\begin{aligned} 0 &= [\partial_{q_c} \tilde{\beta}_0 j(q_c)/2]_{\alpha_3=\beta_1=0} \\ &= \frac{3\tilde{\alpha}_2^2}{2} \left(\frac{2\tilde{\alpha}_0}{3\tilde{\alpha}_2} - (q_c - q_0)^2 \right). \end{aligned} \quad (23)$$

Accordingly, $|q_c - q_0|$ scales as $\sqrt{T_c - T}$, as is the inverse of the coherence length. Thus, the reciprocal critical current is given by

$$\begin{aligned} [j_{c+}]_{\alpha_3=\beta_1=0} &= [-j_{c-}]_{\alpha_3=\beta_1=0} \\ &= \frac{4\sqrt{6}\tilde{\alpha}_2}{9\tilde{\beta}_0} \tilde{\alpha}_0^{3/2}. \end{aligned} \quad (24)$$

Note that this coincides with \bar{j}_c up to first order in α_3 and β_1 . Thus, the well-known scaling law $j_c \sim (T_c - T)^{3/2}$ is reproduced for \bar{j}_c .

Let us consider the first-order change caused by α_3 and β_1 . We obtain

$$\begin{aligned} \partial_{\alpha_3} [\tilde{\beta}_0 j(q)/2] \Big|_{\alpha_3=\beta_1=0} \\ = \frac{5\tilde{\alpha}_2(q - q_0)^2}{12} \left(\frac{6\tilde{\alpha}_0}{5\tilde{\alpha}_2} - (q - q_0)^2 \right), \end{aligned} \quad (25)$$

and

$$\begin{aligned} \partial_{\beta_1} [\tilde{\beta}_0 j(q)/2] \Big|_{\alpha_3=\beta_1=0} \\ = \frac{5\tilde{\alpha}_2^2}{8\tilde{\beta}_0} \left((q - q_0)^2 - \frac{2\tilde{\alpha}_0}{\tilde{\alpha}_2} \right) \left((q - q_0)^2 - \frac{2\tilde{\alpha}_0}{5\tilde{\alpha}_2} \right). \end{aligned} \quad (26)$$

When the critical current j_{c+} is realized at $q_{c+} = q_c + \delta q_c$, we obtain up to first order in α_3 and β_1 ,

$$\begin{aligned} j(q_{c+}) &= [j + \delta j](q_c + \delta q_c) \\ &= j_{c0} + \alpha_3 [\partial_{\alpha_3} j(q_c)]_{\alpha_3=\beta_1=0} \\ &\quad + \beta_1 [\partial_{\beta_1} j(q_c)]_{\alpha_3=\beta_1=0} \\ &\quad + [\partial_{q_c} j(q_c)]_{\alpha_3=\beta_1=0} \delta q_c \\ &= j_{c0} + \alpha_3 [\partial_{\alpha_3} j(q_c)]_{\alpha_3=\beta_1=0} \\ &\quad + \beta_1 [\partial_{\beta_1} j(q_c)]_{\alpha_3=\beta_1=0}. \end{aligned} \quad (27)$$

Here, j_{c0} represents $[j(q_c)]_{\alpha_3=\beta_1=0}$. Thus, we obtain the non-reciprocal component of the critical current,

$$\begin{aligned} \Delta j_c &= 2\alpha_3 [\partial_{\alpha_3} j(q_c)]_{\alpha_3=\beta_1=0} + 2\beta_1 [\partial_{\beta_1} j(q_c)]_{\alpha_3=\beta_1=0} \\ &= \frac{16\tilde{\alpha}_0^2}{27\tilde{\beta}_0\tilde{\alpha}_2} \alpha_3 - \frac{8\tilde{\alpha}_0^2}{9\tilde{\beta}_0^2} \beta_1. \end{aligned} \quad (28)$$

This scales as $\Delta j_c \sim (T_c - T)^2$.

CALCULATION DETAILS AND PHASE DIAGRAMS

Here we explain the details of the numerical calculations and show some additional figures related to the phase diagrams. All the calculations for the figures in the main text and those presented here are done with $L_x = 6000$ and $L_y = 200$. Exceptionally, we adopt $L_x = 12000$ for Fig. 5 and $T > 0.03$ in Fig. 2 to reduce the finite-size effect. To obtain $j_{c\pm}$, $j(q)$ is maximized/minimized among $q \in 2\pi\mathbb{Z}/L_x$. The normalization of Figs. 5 (a)-(d) is done with $\max[j_{c+}, |j_{c-}|]$, $|\min_q F(q)|$, and $\max[0.003, \max_q \Delta E(q)]$ for $j(q)$, $F(q)$, and $\Delta E(q)$, respectively. Note that we show in Figs. 5 (a)-(d) only the most stable state that minimizes $F(q)$ for each q . In particular, there is a metastable superconducting state for smaller (larger) q 's of the left (right) peaks in Fig. 5 (d). The supercurrent sustained by these states might be observed when the experimental time scale is small. For Figs. 5 (a)-(d), it is confirmed that the superconducting solution is (if any) unique for each q .

In Figs. 6 (a) and (b), we show the temperature and magnetic-filed dependence of the minimum excitation energy $\Delta E(q_0)$ for $t_2 = 0$ and 0.2, respectively. The spectrum becomes gapless in the high-field helical superconducting states, which can be detected by scanning tunneling microscopy. Figures 6 (c) and (d) show q_0 and r for $t_2 = 0.2$. In Figs. 6 (c) and (d), the crossover line is seen to be $h \sim 0.17$, and a huge nonreciprocal nature $r \sim 0.8$ is observed. To be precise, Δj_c becomes positive in a tiny region near $h \sim 0.19$ and $T \sim 0$ for $t_2 = 0.2$. However, this is probably due to the peculiarity of the model, where the Lifshitz transition of the outer Fermi surface occurs around $h \sim 0.185$.

EVOLUTION OF LANDAU CRITICAL MOMENTA

As discussed in the main text, the sign reversal of Δj_c by t_2 can be understood based on the nonreciprocity of the Landau critical momenta. In Fig. 7, we show $q_R + q_L$ and q_0 obtained from $j(q)$ at $h = 0.03$ and $T = 0.001$, with varying t_2 from 0 to 0.2. The sign reversal of $q_R + q_L - 2q_0$ (red closed circles) naturally explains that of Δj_c . For large values of t_2 , $q_R + q_L - 2q_0$ is dominated by the nonreciprocal Landau critical momentum $q_R + q_L$ (blue closed triangles), while it is dominated by q_0 (black closed squares) for small values of t_2 . It should be noted that a large SDE is obtained for $t_2 \sim 0.2$, although $q_R + q_L$ and $-2q_0$ contribute destructively.

To understand the behavior of $q_R + q_L$, we discuss the Landau critical momenta with the help of the single-band formula $|\mathbf{q} \cdot \mathbf{v}/2| = \Delta$. In our case, \mathbf{q} should be replaced with $\mathbf{q} - \mathbf{q}_\chi(\mathbf{k})$

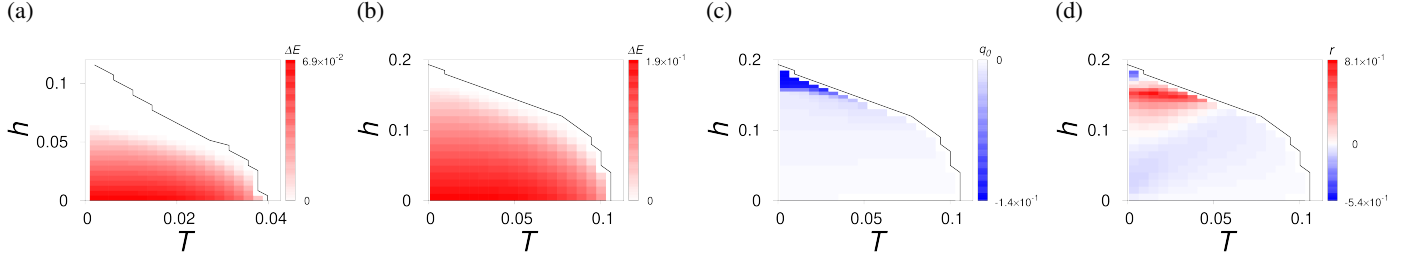


FIG. 6. Temperature and magnetic-field dependence of (a),(b) ΔE , (c) q_0 , and (d) r . $t_2 = 0$ for the panel (a), while $t_2 = 0.2$ for the panels (b)-(d).

for each band, and we obtain,

$$\begin{aligned} \Delta &= \max_{\chi=\pm, \mathbf{k}=\mathbf{k}_F^\chi} \left| \frac{q \hat{x} - \mathbf{q}_\chi(\mathbf{k})}{2} \cdot \mathbf{v}_\chi(\mathbf{k}) \right| \\ &= \max_{\chi=\pm, \mathbf{k}=\mathbf{k}_F^\chi} |qv_{\chi,x}(\mathbf{k})/2 - \chi h \hat{g}_y(\mathbf{k})|, \end{aligned} \quad (29)$$

whose positive and negative solutions for q correspond to q_R and q_L , respectively. Here, \mathbf{k}_F^χ specifies the \mathbf{k} points on the Fermi surface with the helicity χ , while $\hat{g}(\mathbf{k})$ is the unit vector parallel to $\mathbf{g}(\mathbf{k})$. Equation (29) well reproduces the result for $q_R + q_L$, as shown by skyblue open triangles in Fig. 7. To go further, let us simplify the expression by replacing $\mathbf{q}_\chi(\mathbf{k})$ in the first line of Eq. (29) with its average on the Fermi surface: $q_\chi \hat{x} \equiv \langle \mathbf{q}_\chi(\mathbf{k}_{F,\chi}) \rangle$. We obtain for $h > 0$ [see the next section for the derivation],

$$q_R + q_L = \begin{cases} q_+ + q_- \\ + 2 \left(\frac{\Delta}{v_-} - \frac{\Delta}{v_+} \right), & (|\delta v|/\bar{v} \lesssim h/\Delta) \\ 2q_+, & (\delta v/\bar{v} \gtrsim h/\Delta) \\ 2q_-, & (\delta v/\bar{v} \lesssim -h/\Delta) \end{cases} \quad (30)$$

whose helicities are interchanged for $h < 0$. Here, we defined $v_\chi \equiv \max_{\mathbf{k}_F^\chi} v_{\chi,x}(\mathbf{k}_F^\chi)$, $\delta v = v_+ - v_-$ and $\bar{v} \sim (v_+ + v_-)/2$. Equation (30) qualitatively agrees with $q_R + q_L$ for $t_2 \lesssim 0.15$, as shown by the open purple inverted triangles in Fig. 7. In this regime, we have small δv and the first line of Eq. (30) is applied. Since $q_\pm \sim \pm 2h/v_\pm$, the difference of the Fermi velocities δv plays a key role to obtain a large $q_R + q_L$. It is expected that the anisotropy of the system is advantageous to obtain a large value of δv . On the other hand, Eq. (30) underestimates $q_R + q_L$ around $t_2 = 0.2$, where the third line of Eq. (30) is applied. This indicates that the isotropic simplification $\mathbf{q}_\chi(\mathbf{k}) \rightarrow q_\chi \hat{x}$ is not valid for strongly anisotropic systems with large t_2 . Thus, overall, large anisotropy of the system is expected to be the key to obtain a large SDE.

In Fig. 8, we show the magnetic-field dependence of $q_R + q_L$, q_0 and their combinations for $t_2 = 0.2$. The notations are the same as those of Fig. 7. While $q_R + q_L$ is nonmonotonic, $-2q_0$ grows linearly and finally the sign reversal of $q_R + q_L - 2q_0$ occurs. “ $q_R + q_L$ (aniso)”, i.e. Eq. (29), qualitatively captures the behavior of $q_R + q_L$, whose slight deviation is probably due to the higher-order corrections of h . The

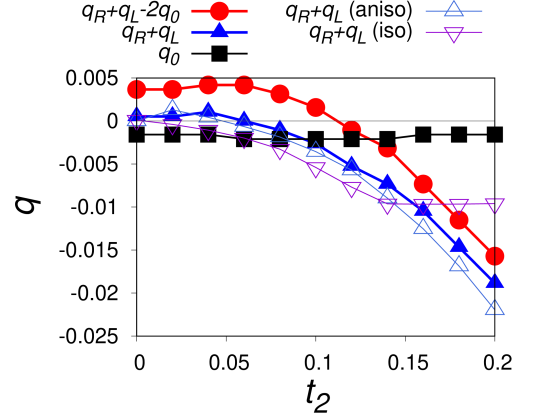


FIG. 7. t_2 dependence of $q_R + q_L$, q_0 , and their combinations. The red closed circles, blue closed triangles, black closed squares indicate $q_R + q_L - 2q_0$, $q_R + q_L$, q_0 evaluated from $j(q)$, respectively. The open sky-blue triangles and open purple inverted triangles indicate $q_R + q_L$ calculated from Eq. (29) and that with the isotropic simplification $\mathbf{q}_\chi(\mathbf{k}) \rightarrow q_\chi \hat{x}$, respectively.

isotropic simplification does not work for $t_2 = 0.2$ as is clear in Fig. 8. The sign reversal of $q_R + q_L - 2q_0$ is the origin of that of Δj_c in the phase diagram for $t_2 = 0.2$ under moderate magnetic fields.

Derivation of Eq. (30)

Here, we derive Eq. (30). By using $\mathbf{q}_\chi(\mathbf{k}) \rightarrow q_\chi \hat{x}$, we obtain

$$2\Delta = \max_{\chi=\pm} \left[|q - q_\chi| \max_{\mathbf{k}_F^\chi} |v_{\chi,x}(\mathbf{k})| \right] \quad (31)$$

$$= \max_{\chi=\pm} \left[|q - q_\chi| v_\chi \right]. \quad (32)$$

Let us first consider the positive solution $q = q_R > 0$. We also fix $h > 0$. Then, we obtain

$$2\Delta = \max \left[(q_R + |q_-|)v_-, (q_R - |q_+|)v_+ \right]. \quad (33)$$

When $(q_R + |q_-|)v_- > (q_R - |q_+|)v_+$, we obtain

$$q_R = q_- + \frac{2\Delta}{v_-}. \quad (34)$$

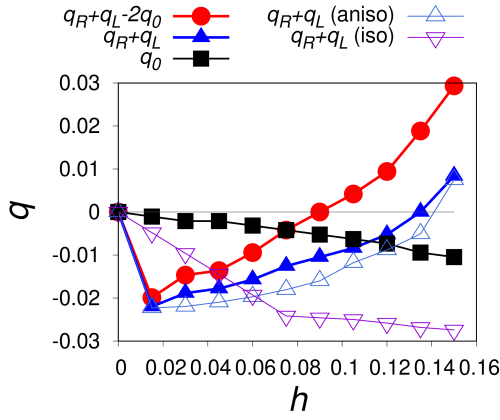


FIG. 8. Magnetic field dependence of $q_R + q_L$, q_0 and their combinations for $t_2 = 0.2$ and $T = 0.001$. The notations are the same as Fig. 7.

The consistency can be checked as follows. The above inequality reads

$$\delta v q_R < |q_-|v_- + |q_+|v_+ \sim 2h. \quad (35)$$

Thus, this solution is valid for

$$2h \gtrsim \delta v \frac{2(\Delta - h)}{v_-} \sim \frac{2\delta v(\Delta - h)}{\bar{v}}. \quad (36)$$

Considering only the linear dependence in h , we obtain

$$q_R = q_- + \frac{2\Delta}{v_-}, \quad \frac{\delta v}{\bar{v}} \lesssim \frac{h}{\Delta}. \quad (37)$$

In the same way, we obtain

$$q_R = q_+ + \frac{2\Delta}{v_+}, \quad (38)$$

for $\delta v q_R \gtrsim 2h$, i.e. $\delta v/\bar{v} \gtrsim h/\Delta$. The negative solutions $q = q_L < 0$ are obtained as follows:

$$q_L = \begin{cases} q_+ - \frac{2\Delta}{v_+}, & \frac{\delta v}{\bar{v}} \gtrsim \frac{h}{\Delta} \\ q_- - \frac{2\Delta}{v_-}, & \frac{\delta v}{\bar{v}} \lesssim \frac{h}{\Delta} \end{cases} \quad (39)$$

Summing up q_R and q_L , we obtain Eq. (30).